plastic preform and over-mold them with the discontinuous fiber-reinforced material, resulting in a structural part that is much lighter, tougher, and stronger than the traditional single material steel components it replaces.

Hybrid parts have been particularly important in the automotive industry. One of the first hybrid structures was the front end of the Audi A6 in 1998, which lowered the cost by 10% and the weight by 15% [25]. In 1999, Ford introduced the hybrid front end for their Focus, making it 40% lighter and 20% cheaper than the steel part it replaced. This front end integrated steel inserts over-molded with 30% glass fiber filled polyamide 6 features. The front end is depicted in Figure 1.12.

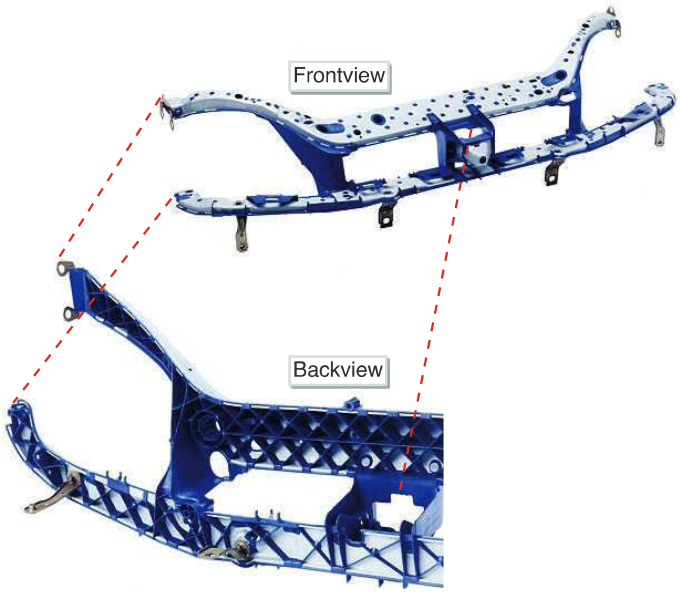

Figure 1.12 Ford-Focus hybrid front end structure made of steel inserts over-molded with 30% by weight glass reinforced polyamide 6 (Courtesy Dynamit Nobel Kunststoff)

1.3 Lightweighting in Automotive Applications

In recent years, global temperatures have been rapidly rising, pushing noticeable changes in the environmental patterns and landscape, including sea levels. At this moment, the earth environment is still relatively stable. However, many scientists fear that, if the current trends continue, the environment may reach a tipping point where significant irreversible shift in the earth environment may be triggered,

causing large changes in the landscape and human disaster of unknown proportions. There are many theories on what is causing the global warming. The majority of the scientist believes that the increased emission of carbon dioxide from the fossil fuels such as petroleum, natural gas, and coal are major contributors. In the past 100 years, since the advent of industrial revolution, the use of such fossil fuels has grown tremendously (9 kTWh in 1910 to 123 kTWh in 2010) due to the increase in population and changes in the lifestyle.

Automobiles in the U.S. are considered among the largest emitters of carbon dioxide. As shown in Figure 1.13, almost 28% of greenhouse gases are coming from transportation. This directly correlates with the energy consumption in the transportation sector at 28% of the total energy consumed in the U.S., as shown in Figure 1.14. Therefore, it is imperative that we reduce the fuel consumption in the transportation industries to lower the greenhouse gases overall.

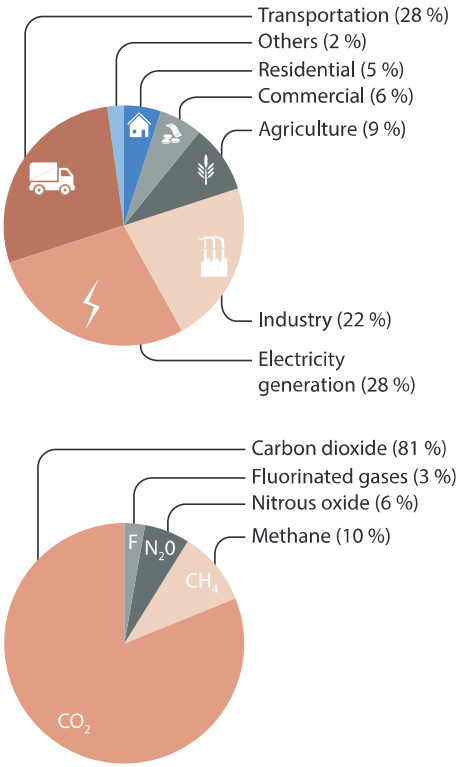

Figure 1.13 Source and breakdown of content of greenhouse gases in the U.S.; note that 28% of greenhouse gases are coming from transportation [7]

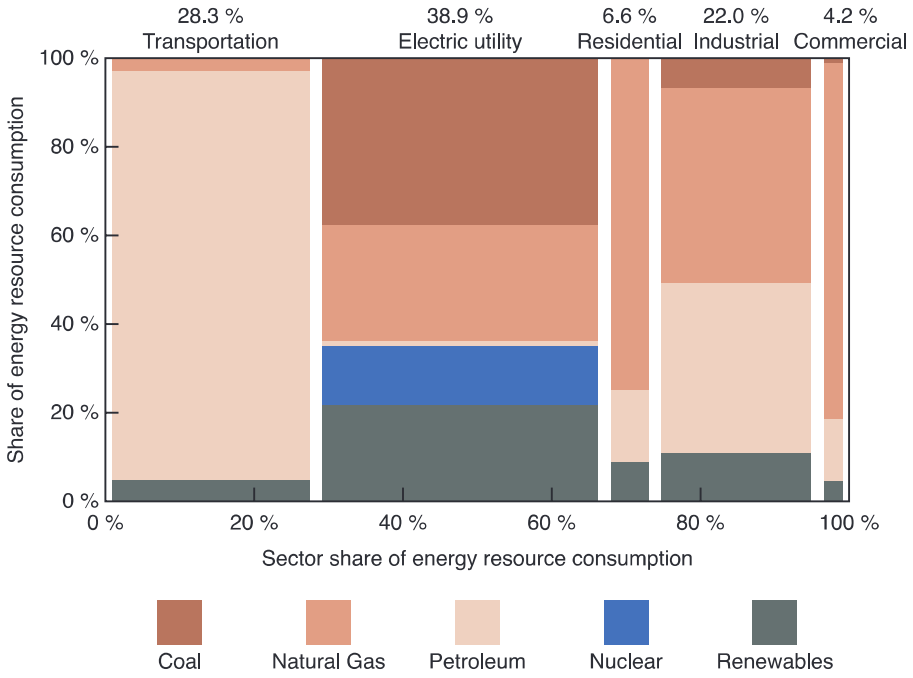

Figure 1.14 U.S. energy consumption by sector; 28% of the energy is consumed by transportation sector; most of it comes from petroleum [8]

The fuel consumption can be reduced by improving the powertrain efficiency, reducing the aerodynamic drag, and using lighter vehicles. Many studies conducted over time in the U.S. [9–11] indicate that for every 10 percent reduction in vehicle weight, fuel consumption can be reduced by approximately 4–8 percent. Actual reduction can vary based on the vehicle specifics, but the trend holds true in general. The main reason for such a direct relationship is engine size. As the vehicle weight is reduced, the power to accelerate the vehicle is also reduced; hence, smaller engines are needed. The smaller engine size becomes the key contributor in reducing the fuel consumption. When the vehicle body is made of lighter materials to reduce weight, it has cascading effects; the size and weight of auxiliary components such as brakes, wheel axles, transmission, and engine are reduced as smaller amounts of weight are supported. As a result, for an engine operating under similar conditions, it can be smaller and use less fuel. The flow of energy from fuel is presented in Figure 1.15: almost 2/3 of energy is used in the engine, while the remaining energy is used in overcoming the friction and other losses; only about 10–12 percent of the energy goes into moving the vehicles. The weight reduction is even more important for electric vehicles. This is because as the vehicle's weight is reduced the energy required to travel is also reduced, hence realizing significant improvements in the range [12].

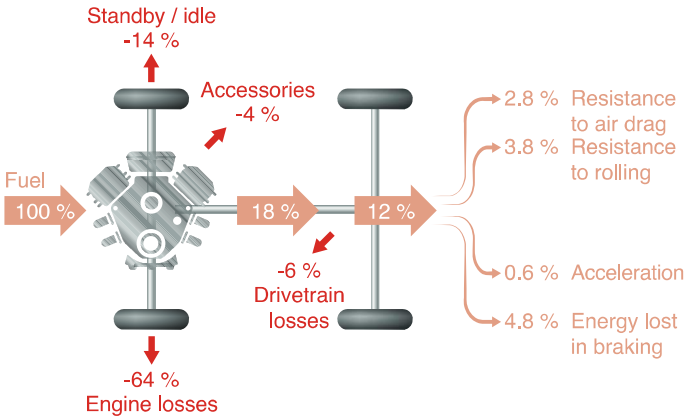

Figure 1.15 Source of fuel usage in a typical vehicle and how weight reduction can help

Therefore, weight reduction of the vehicle body structure has become one of the key focus areas. The history of a typical passenger vehicle's weight since 1975 is presented Figure 1.16. It is interesting to observe that after the fuel crisis in the late 1970s the vehicles became significantly lighter in the early 1980s and then the weight started to increase. Trends in the past 10 years show that the weight of vehicles have stabilized. If we consider the Toyota Corolla, a typical Corolla that weighed about 950 kg in 1983 increased its weight to 1350 kg in 2010. The increase in the vehicle weight was due to many safety regulations rolled out in the 1990s and 2000s, which resulted in improvements in the vehicle structure to absorb crash energy, sensors to detect the impact, and airbags to protect the occupants. These all improved safety but also added weight to the car. In addition, the demand for more comfort and entertainment has increased significantly in the past few years, resulting in larger vehicles with many comfort features and gadgets. During the same period the powertrain technology has also significantly improved. Surprisingly, the result is that the fuel consumption per mile has only increased modestly. In recent years (since 2005) we observe that the weight increase has stabilized while technology to improve fuel efficiency continues to improve; as a result, fuel economy has continued to improve [13].

2 Materials

The major components of a composite material are the reinforcing phase and the surrounding matrix. The reinforcing phase can be particles, agglomerates, platelets, or fibers. When considering fibers, they are either continuous or discontinuous while the continuous fibers can also be woven or braided. In general, the reinforcing phase is joined to the matrix with sizing materials, which depend on the type of matrix used, which can be either thermoplastic or thermosetting. This chapter will present an overview of the reinforcing phase and the matrix.

2.1 Reinforcing Phase

Composite materials are a distinctive set of materials characterized by the combination of individual components to achieve an enhanced material, which exceeds the capabilities of each individual phase. Due to the unique properties of composites, these materials are found in many industries and unique processes have been developed that correspond to the various types of reinforcement. In their most general form, composites are the result of embedding particles of one material in a surrounding matrix of another material. The combination of the particles with the matrix produces a favorable mix of properties that cannot be achieved with either of the constituents acting alone. There are many types of composite materials and Figure 2.1 presents a general classification of fiber-reinforced composites. The shape and dimensions of the reinforcing phase highly affect the mechanical properties of the composite and, in general, composite materials are classified based on the geometry of the reinforcement.

Figure 2.1 is only one way of classifying fiber-reinforced composite materials and a more general and comprehensive classification can include non-fibrous particles or hybrid compositions. Within the larger classification of fibers we can subdivide those as continuous and discontinuous fibers.

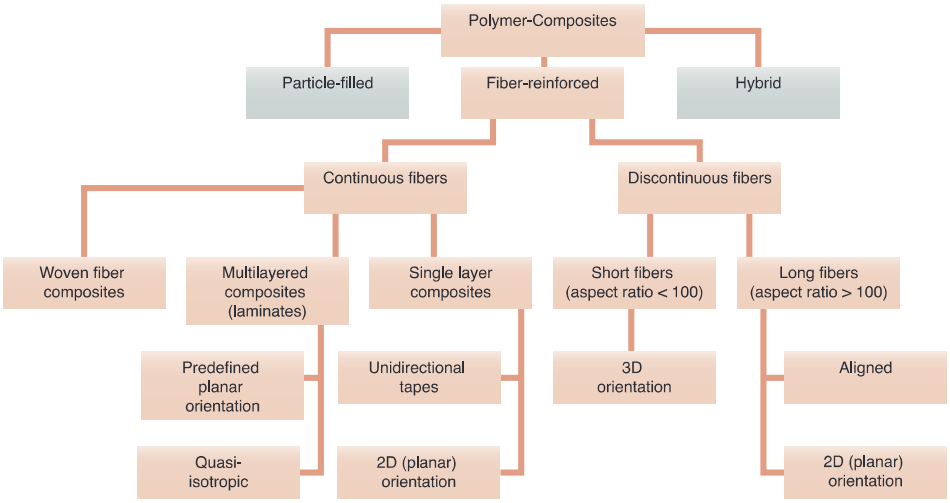

Figure 2.1 Classification of composite materials based on the type of reinforcement

2.1.1 Particle-Reinforced Composites

Particles are those reinforcing materials that do not have a long dimension and can have a spherical, ellipsoidal, obloidal, polyhedral, or even irregular shape. Particle-reinforced composites are some of the oldest types of composite materials. Particulate fillers can increase the stiffness of composite parts, but the level of reinforcement is much smaller than that of fiber-reinforced composites, as the small particles lead to stress concentrations that make the combined materials brittle. For example, a polymer that is tough in its unfilled state becomes brittle when volume fractions of the particles exceed 10% [1]. More often, particles are used to enhance properties such as thermal and electrical conductivity, surface hardness, and wear resistance. The most popular particle used in particle-filled polymers is carbon black. This inorganic filler has been used in the rubber industry since the advent of the rubber tire in the form of rubber/carbon-black composites. Carbon-black, which when dispersed is composed of 10 nm to 100 nm particles, serves not only to stiffen and reinforce rubber, but also to increase its thermal and electrical conductivity. Besides enhancing the properties of the composite, particles can be considerably cheaper than the matrix material. Thus, particles can also be simply used to reduce cost. In the field of inorganic particulate fillers, an active research area in the composites industry has emerged, which concentrates on making polymers more thermally conductive, in some cases by a factor of 100 [2]. This allows the use of inexpensive manufacturing techniques to mold particle-filled plastic parts that conduct heat out of critical automotive components, computers, and heat exchangers [3] as well as in mechatronics applications.

A new class of particle-reinforced composites, nanocomposites, has its roots in the rubber industry. By definition, nano-sized particles have at least one dimension in the nanometer scale. The nano-fillers have an exceptionally high surface to volume ratio and, compared to their bulk size equivalents, nanoparticles have significantly different properties. Nanoparticles greatly improve the properties of the composite and sometimes only small amounts of nanoparticles can lead to improved performance.

Although particle-reinforced composites are a major class of composites, the discussion in this chapter focuses on fiber-reinforced polymer composites. For a detailed discussion on particle-filled composites, the authors suggest [4].

2.1.2 Continuous Fibers

Continuous fiber-reinforced composites are used in structural applications where increased strength and stiffness are required. For example, by stacking single plies of continuous fibers, composites are often made into laminates. The fibers in each ply have a defined orientation and the arrangement of the plies is tailored to enhance the strength of the composite in the primary load directions. For continuous fiber-reinforced composites, the orientation of the fibers is pre-defined by assembling preforms and typically does not change during processing. Several identical or different layers may be bonded together, which is also referred to as *laminate*. The orientation of the fibers in each layer is designed to match the load of the final part. Such types of continuous fiber composites have been traditionally used in aerospace applications, such as in the Boeing 787 discussed in Chapter 1, as well as in lower volume production automobiles such as some panels and structural elements like the B-pillar of the R8 Audi Super sports car, also presented in Chapter 1.

Textile composite structures are an advanced subcategory of continuous fiber composites, which can even further improve the performance of a composite part. The three main types of fabric used in textile composites are: woven, braided, and knitted. Knitted fabric results from knitting of fibers. Generally, such fabrics are stretchable with low tensile and compressive properties, which makes them ideal for gloves, shoes, etc. Their usage in composites has been limited so we will focus on the other two types in the next section.

2.1.2.1 Woven Fabrics

Resin impregnated woven fabrics are widely used in hybrid structures, where they are over-molded with discontinuous fiber-filled ribbed structures. The simplest form of a woven fabric is the one that has a plain weave and is schematically depicted in Figure 2.2 (left). In a weave, the longitudinal threads are called the warp,

and the lateral threads are called the weft or the filling. A woven fabric is typically manufactured using a loom that interlaces the warp and weft yarns. The longitudinal threads, or warp threads, are held stationary and in tension, and the weft or fill is inserted over and under the warp threads.

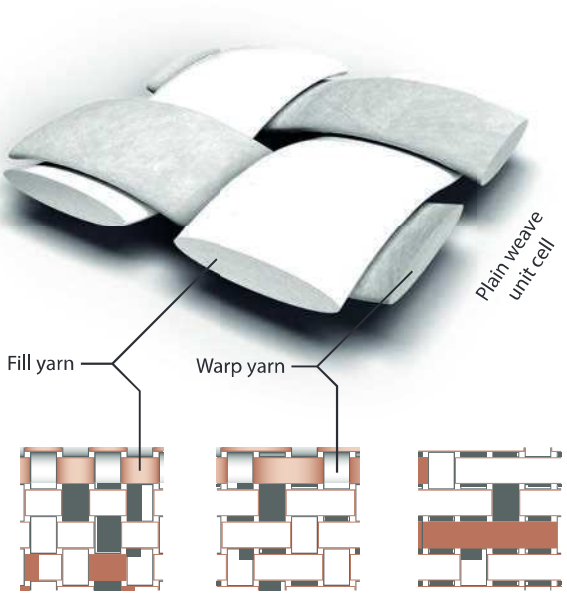

Figure 2.2 Most common types of fabrics: plain (left), twill (center), and satin (right)

Three major types of weaves are used in the composites industry [5]. These are plain, twill, and satin weave. The plain weave is the type of weave with the shortest float where warp and weft are interlaced at every intersection. In a twill fabric, the weft skips or floats over one or more warp threads. A satin is the type of fabric where the weft skips over more than four warp threads. With increasing float, the resistance to deformation decreases, which can have a negative impact when handling the fabric but can improve its drapability. This makes twills and satins more likely to take on shapes that have double curvatures. If the weave of two neighboring weft threads is shifted by one thread, a characteristic diagonal pattern is created such as shown with the twill and satin weaves in Figure 2.2 (center and right) [6].

In the manufacture of hybrid structures, woven fabrics must often be conformed to complex three-dimensional surfaces such as shown in Figure 2.3. The figure depicts an X-ray micro-computed tomography (μCT) scan as an example of a thermoplastic impregnated fabric, draped over a complex tool. As can be seen, such a draping process poses many problems such as those resulting from wrinkling and

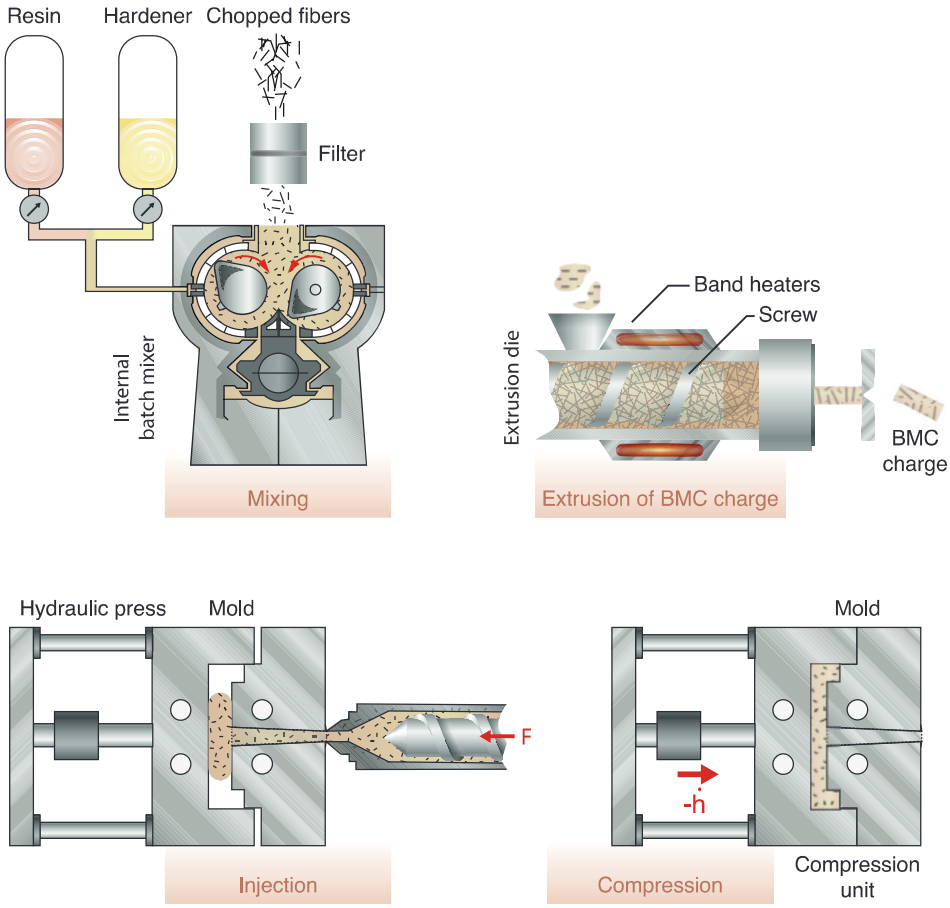

Figure 3.6 BMC injection-compression molding process

■ 3.2 Fiber-Reinforced Thermoplastics

In a thermoplastic polymer, the molecules are not cross-linked with each other. Instead, the individual molecules are held in place by weaker intermolecular forces such as van der Waals forces and hydrogen bonds. In polymer processes, thermoplastics solidify as they are cooled from the molten state and the long molecules are no longer allowed to move freely. When reheated, these materials regain the ability to "flow" and the molecules are able to slide past each other with ease. Thermoplastic polymers are divided into two classes: amorphous and semi-crystalline polymers. Amorphous thermoplastics have molecules that remain in disorder as they cool, leading to materials with a fairly random molecular structure. An

amorphous polymer hardens, or vitrifies, as it is cooled below its glass transition temperature. Semi-crystalline thermoplastics, on the other hand, solidify while forming a crystalline structure. As the material is cooled, the molecules begin to arrange in a regular order once the temperature drops below the melting temperature. However, in semi-crystalline polymers small amorphous regions remain where the molecules are not ordered. These amorphous regions within the semi-crystalline domain lose their "flowability" below their glass transition temperature. Because most semi-crystalline polymers have a glass transition temperature at subzero temperatures, they behave like rubbery or leathery materials at room temperature.

Discontinuous fiber-reinforced thermoplastics have been used in injection or compression molding for a long time. Compared to SMC or BMC, fiber-reinforced thermoplastics show advantages such as higher impact strength, lower cycle times, and recyclability. However, the high viscosity of a thermoplastic resin makes it more difficult to impregnate the fibers and the surface finish is poor compared to SMC. Different processes have been developed and several material combinations exist. Depending on the application, the matrices may be of polypropylene, polyamide, or any other engineering thermoplastic. Currently, glass fibers have the biggest market share, although the applications with carbon fibers are increasing. The following sections summarize the three main processes in discontinuous fiber-reinforced thermoplastics: injection molding, compression molding, and extrusion-compression molding.

3.2.1 Injection Molding

Injection molding is the most important process used to manufacture plastic products. Today, more than one-third of all thermoplastic materials are injection molded and more than half of all polymer processing equipment is for injection molding. The injection molding process is ideally suited to manufacture mass-produced parts of complex shapes requiring precise dimensions. The process goes back to 1872, when the Hyatt brothers patented their stuffing machine to inject cellulose into molds. However, today's injection molding machines are mainly related to the reciprocating screw injection molding machine patented in 1956. A modern injection molding machine with its most important elements is shown in Figure 3.7. The components of the injection molding machine are the plasticating unit, clamping unit, and the mold.

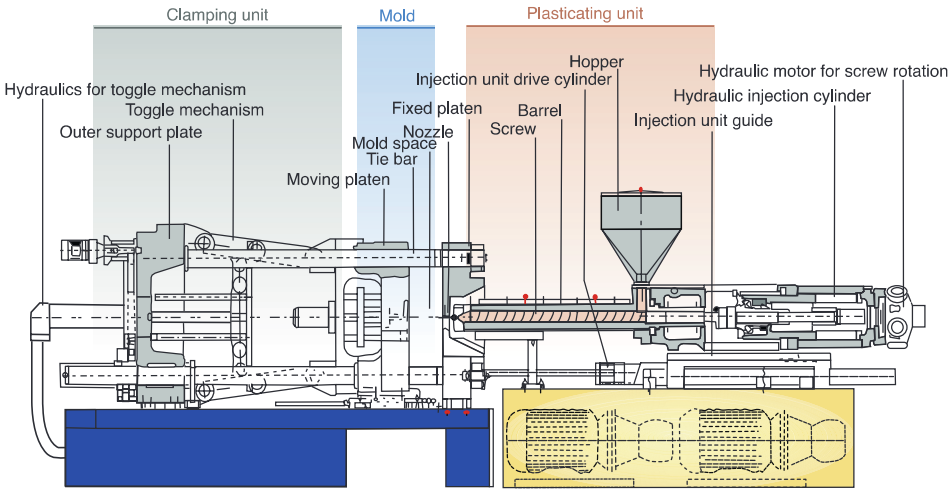

Figure 3.7 Schematic of an injection molding machine

Today, injection molding machines are classified by the following international convention[1]

$$\text{Manufacturer } T / P \tag{3.1}$$

where T is the clamping force in metric tons and P is defined as

$$P = \frac{V_{\max} p_{\max}}{1000} \tag{3.2}$$

where $V_{\max}$ is the maximum shot size in cm^3 and $p_{\max}$ is the maximum injection pressure in bar. The clamping force T can be as low as 1 metric ton for small machines, and as high as 11,000 tons.

The sequence of events during the injection molding of a plastic part, as shown in Figure 3.8, is called the injection molding cycle. The cycle begins when the mold closes, followed by the injection of the polymer into the mold cavity. Once the cavity is filled, a holding pressure is maintained to compensate for material shrinkage. In the next step, the screw turns, feeding the next shot to the front of the screw. This causes the screw to retract as the next shot is prepared. Once the part is sufficiently cool, the mold opens and the part is ejected.

[1] The old U. S. convention uses Manufacturer *T-v*, where *T* is the clamping force in British tons and *v* the shot size in ounces of polystyrene.

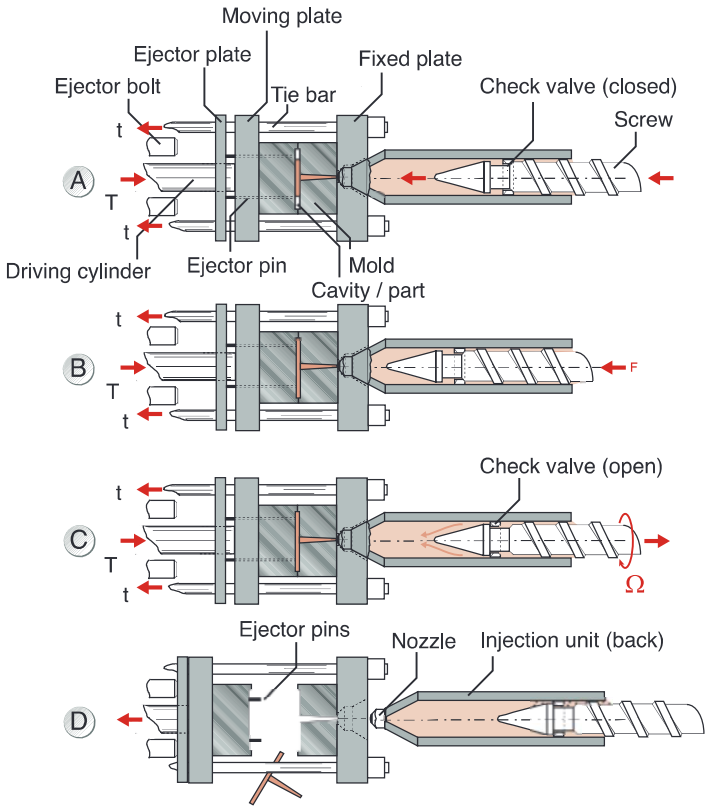

Figure 3.8 Sequence of events during an injection molding cycle

Figure 3.9 schematically illustrates the sequence of events during the injection molding cycle. The figure shows that the cycle time is dominated by the cooling of the part inside the mold cavity. The total cycle time can be calculated using

$$t_{\text{cycle}} = t_{\text{closing}} + t_{\text{cooling}} + t_{\text{ejection}} \tag{3.3}$$

where the closing and ejection times, t_{closing} and t_{ejection}, can last from a fraction of a second to a few seconds, depending on the size of the mold and machine. The cooling times, which dominate the process, depend on the maximum thickness of the part. The cooling time for a plate-like part of thickness h can be estimated using

$$t_{\text{cooling}} = \frac{h^2}{\pi\alpha} \ln\left(\frac{8}{\pi^2}\frac{T_m - T_w}{T_D - T_w}\right)$$

and for a cylindrical geometry of diameter D using

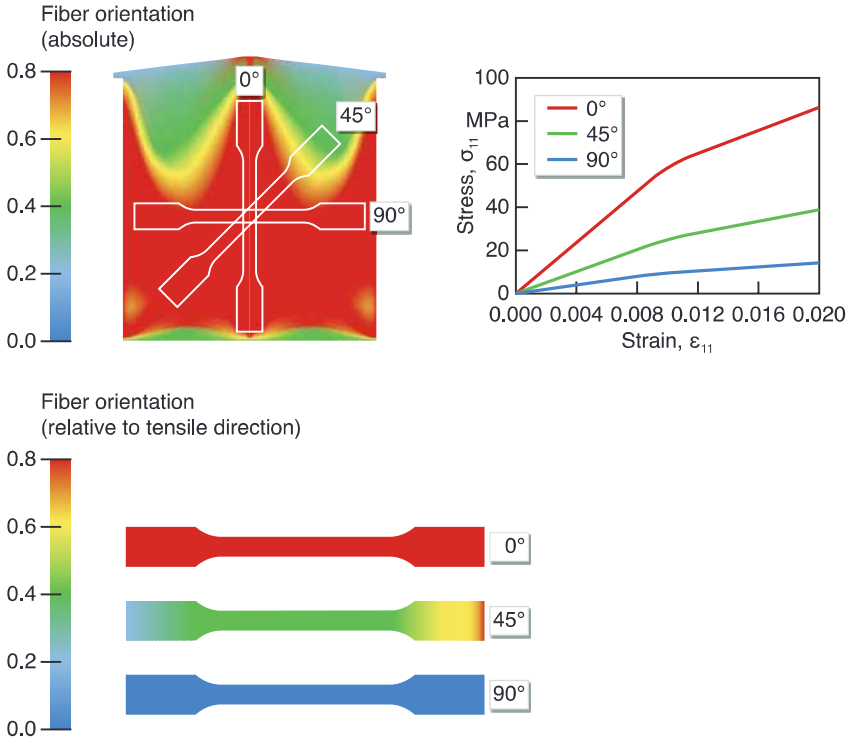

Figure 4.14 Illustration of the process-induced fiber orientation, obtained from a basic process simulation of a fan-gated plaque. The impact of fiber orientation, caused by the mold filling, is shown for specimens extracted at 0, 45, and 90 degrees

For a more detailed discussion on process simulation, the reader should consult Chapter 7 of this book. Furthermore, the effect of process-induced microstructure on the mechanical properties within a plaque is investigated in detail in Chapter 8.

■ 4.2 Characterization Techniques for Fiber Microstructure Analysis

Quantifying the process-induced fiber configuration in molded samples is of utmost importance so that the underlying physics of the process–microstructure relationship can be studied experimentally. Furthermore, accurate and reliable experimental data are required to test and develop numerical models and predictive tools. At times, the lack of accurate experimental data limits the progress of validating modeling approaches [2, 6]. Nevertheless, the characterization of fiber configuration is a cumbersome task since even small samples comprise millions of fi-

bers. A wide variety of measurement approaches exist, but no standard has been accepted nor has a uniform procedure been defined. While some measurement concepts share similarities, there are substantial differences in key aspects of the measurement techniques and the execution of the actual measurements. The following sections provide an in-depth review and discussion of measurement techniques used to quantify the orientation, length, and concentration in discontinuous fiber-reinforced polymers.

4.2.1 Measuring Fiber Orientation

For decades, fiber orientation measurements were performed manually by physically sectioning the sample and inspecting the cross sections using optical reflection microscopy [45–47], which is referred to as the method of ellipses (MoE). The fibers leave elliptical footprints on the polished cross sections, which are detected and analyzed for individual fibers. The fiber orientation can be quantified by analyzing the shapes of the ellipses, as illustrated in Figure 4.15. An image analysis system imports the captured micrographs and fits ellipses to determine the angles ϕ and θ individually for each fiber [47]. Although newer systems are automated to a degree, this technique still requires a lot of manual work to achieve accurate results. Furthermore, the destructive nature of this method does not allow additional testing of the sample, e.g., fiber length analysis. Moreover, the two-dimensional observation of the ellipses results in ambiguity with respect to the out-of-plane angle θ, because the fiber can be oriented at θ or $\theta+\pi$, as illustrated in Figure 4.15. However, this ambiguity can be resolved by an additional etching after each polishing step, so that a fiber's shadow is visible in the micrograph. By determining the location of the shadow relative to the corresponding fiber, the angle θ can be distinctly defined [32].

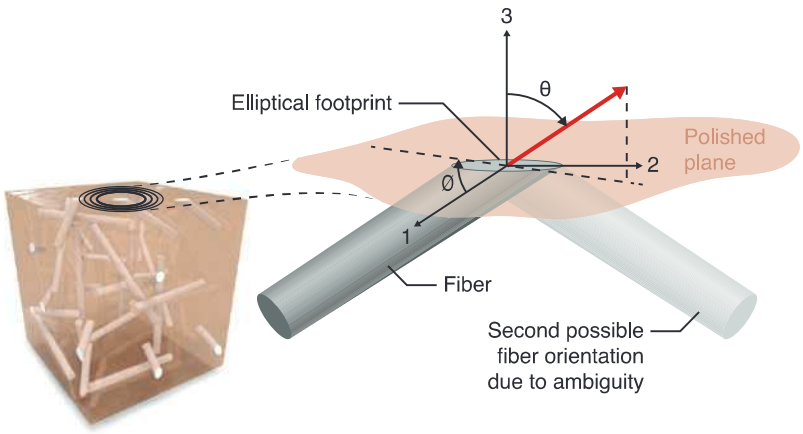

Figure 4.15 Basic principle of the method of ellipses and illustration of the ambiguity in the out-of-plane angle θ

A relatively new approach to measure fiber orientation distribution within fiber-reinforced plastic parts is applying the X-ray micro-computed-tomography (μCT) technology. This technique is a non-destructive testing (NDT) method, which enables a full 3D analysis of a specimen and the quantification of internal material structure [48–50]. The advantage of μCT is that it can achieve high resolution of the full 3D microstructure without destroying the specimen. Originally, μCT was solely used in medical applications, but it has now evolved to be a conventional characterization technique in the material sciences and in industrial applications. A basic schematic of the μCT process is illustrated in Figure 4.16.

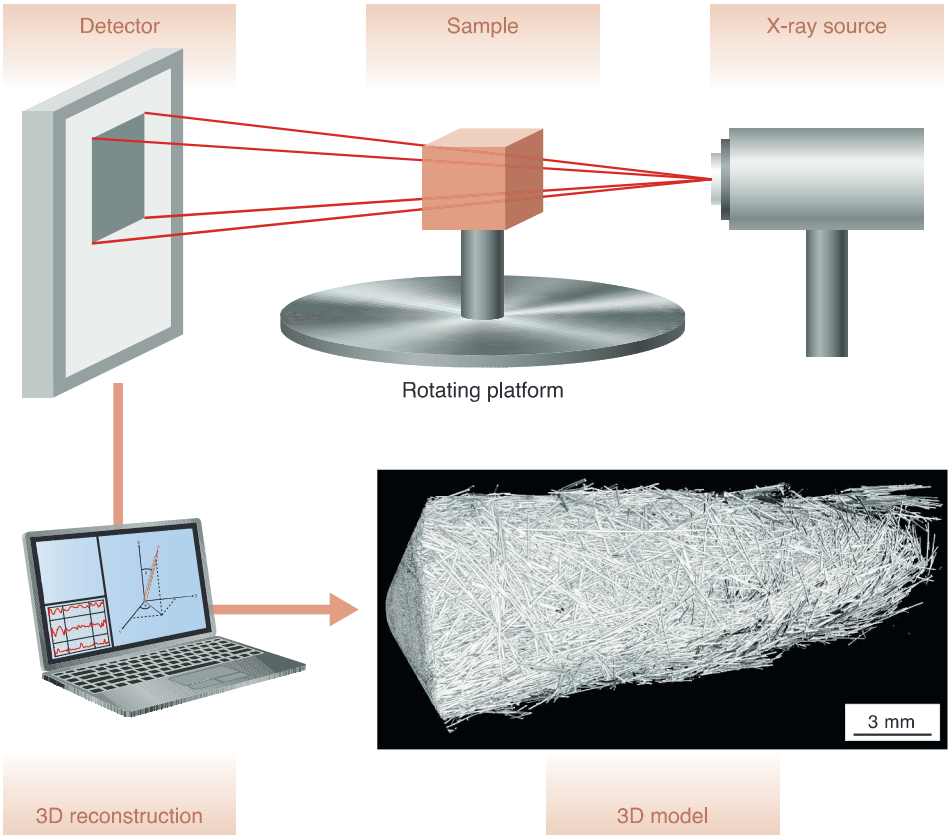

Figure 4.16 Illustration of the X-ray computed-tomography process: the μCT system comprising the detector, X-ray source, and rotating platform (top), the computer-assisted tomographic reconstruction (bottom left), and a 3D rendering of the data reconstruction (bottom right)

In general, the system consists of an X-ray source, a rotating platform and a detector. The basic principle of μCT is to irradiate a sample with penetrating X-rays, which are attenuated and captured downstream of the object with a detector system creating radiographs. At defined energy levels, the X-ray source irradiates the

specimen, which is placed on a rotating platform to achieve a full scan of the sample. The detector records the attenuated X-rays as radiographs at incremental angles during the rotation of the sample. Each captured projection (radiograph) is a two-dimensional intensity distribution of the attenuated X-rays. The intensity distribution is directly related to the material's atomic density. A phase of high atomic density within the specimen absorbs more energy than low-density materials.

The X-rays interact with the sample and are attenuated in various ways. For the energy range of the X-rays used in material science, the most relevant mechanisms are Compton scattering and photoelectric effects [48]. Most fundamentally, the attenuation of an X-ray through a sample can be described by the change in intensity I as

$$dI = -\mu_{eff}(x)I(x)dx \tag{4.11}$$

where μ_{eff} is the effective linear attenuation coefficient and x is the location on the path. Integration of Equation (4.11) along the path C gives

$$-\ln\frac{I}{I_0} = \int_C \mu_{eff}(x)dx \tag{4.12}$$

which is also referred to as the Beer-Lambert law. Computing the correct value of μ_{eff} at each position along the path C is the central problem of computed tomography, called tomographic reconstruction. Several approaches and algorithms exist for the reconstruction and the reader is directed to [48] for more detailed information.

After the completion of the 3D reconstruction, the μCT data set can be further processed for qualitative and quantitative analysis of the actual specimen. Different software and algorithms exist to process the μCT images and analyze the fiber orientation distribution. A major challenge in using μCT for fiber orientation analysis is the amount of data that is generated, which has to be post-processed to quantify the orientation. For example, a scan of a 20 × 20 × 3 mm^3 sample at a resolution of 10 μm results into 8 GB of data. There are software packages from the medical field, e. g., Mimics® (Materialise NV, Belgium) that are adapted to be used for fiber orientation analysis [51]. Another software package for material science and industrial application is VG Studio MAX (Volume Graphics GmbH, Heidelberg, Germany), which also has a module for fiber orientation analysis and quantifies the fiber orientation using the structure tensor approach [52]. It was shown that VG Studio MAX provides fast and accurate μCT data analysis, making it the most commonly used software for fiber orientation measurements at the moment [53]. Additionally, research groups frequently develop their own image processing algorithms to quantify the fiber orientation from μCT scans.

The resolution (voxel size) of the scan is one of the most important parameters that determine the accuracy of the feature analysis of scanned samples. However, the trade-off between scan resolution and sample size needs to be considered. In general, finer scan resolutions require samples with smaller dimensions. Although a very fine resolution might be needed for an accurate analysis, a small sample might not fully represent the local orientation, especially for long fiber-filled materials. It has not been established what the minimum resolution might be to perform an accurate fiber orientation analysis for a specific fiber type. Furthermore, μCT scanning is limited in the case of composite materials with constituents that have similar atomic densities (e.g., carbon fiber-reinforced polyamide) since the contrast of the constituents in the radiograph is low and identifying the fibers can become challenging [80].

There is a wide variety of analysis resolution and sample size used in the microstructure analysis of fiber-reinforced samples throughout reported studies. The sample dimensions range from 3 μm voxel size resolution (sample size: 4 mm disk with a thickness of 4 mm) [54] up to a voxel size of 40 μm (sample size: 40 mm × 40 mm × 30 mm) [55]. To provide the reader an overview of recently published studies that apply fiber orientation measurements, Table 4.1 summarizes the imaging technique, sample size, and resolution used in their work.

Table 4.1 Overview and Summary of Fiber Orientation Measurement Techniques Applied in Recently Published Studies

Material	Imaging Technique	Sample Dimensions	Resolution	Reference
PP/GF	μCT	3 × 3 × 3 mm^3	8.0 μm	[56]
PA66/GF	μCT	3 × 3 × 3 mm^3	2.5 μm	[57]
PP/GF	μCT	16 × 16 × 3 mm^3	6.0 μm	[33]
PA6/GF	μCT	4 × 4 × 2 mm^3	1.4 μm	[49]
PA66/GF	μCT	10 × 10 × 2 mm^3	6.5 μm	[58]
PA6/GF	μCT	3.6 × 3.1 × 3.9 mm^3	9.0 μm	[59]
Natural Fibers	μCT	6 × 6 × 3.5 mm^3	7.8 μm	[60]
PP/GF	μCT	n/a	8.1 μm	[61]
PA66/GF	μCT	5 × 20 × (1 to 3) mm^3	6.0 μm	[62]
PP/GF	μCT	Ø 4 mm and 4 mm thickness	3.3 μm	[54]
PA6/GF	μCT	Ø 4 mm and 4 mm thickness	1.8 μm	[63]
PA/GF	μCT	Ø 4 mm and 4 mm thickness	0.7 μm	[64]
PA6/GF	Cross-sectional polishing and μCT	3.2 × 4 × 15 mm^3	9.0 μm	[65]
PP/GF	Cross-sectional polishing	1.5 × 2 × 1.7 mm^3	0.24 μm	[66]
PP/GF	Cross-sectional polishing	2 × 2 × 0.7 mm^3	n/a	[67]